Hindawi
Advances in Civil Engineering
Volume 2019, Article ID 2572034, 16 pages
https://doi.org/10.1155/2019/2572034

Research Article

Combined Application of Optical Fibers and CRLD Bolts to Monitor Deformation of a Pit-in-Pit Foundation

Chun Zhu,[1,2,3] **Kai Zhang**,[2,3] **Huan Cai**,[4] **Zhigang Tao**,[2,3] **Bo An**,[2,3] **Manchao He**,[1,2,3] **Xing Xia**,[2,3] **and Jiankang Liu**[5]

[1]*College of Construction Engineering, Jilin University, Changchun 130026, China*
[2]*State Key Laboratory for Geomechanics & Deep Underground Engineering, Beijing 100083, China*
[3]*School of Mechanics and Civil Engineering, China University of Mining & Technology, Beijing 100083, China*
[4]*China Gold International Resources Corp. Ltd., China*
[5]*School of Engineering, Nagasaki University, 1-14 Bunkyo-machi, Nagasaki, Japan*

Correspondence should be addressed to Zhigang Tao; taozhigang@263.net

Received 23 October 2018; Revised 28 December 2018; Accepted 13 January 2019; Published 5 February 2019

Academic Editor: Daniele Baraldi

"Pit-in-pit" foundations, where the overall pit is divided into inner and outer pits, present a wide range of engineering problems and yet have received little detailed study. Among the many factors that affect the stability of a deep foundation pit, loading and rainfall are the two most important. Therefore, in this study, physical model experiments are carried out in the laboratory based on a pit-in-pit foundation that is typical of engineering applications in China, simulating the deformation of the system under different loading and rainfall flow conditions. Optical fibers along with constant resistance and large deformation (CRLD) bolts are adopted to collectively monitor the stress and strain inside the pit-in-pit foundation, assisted by fiber Bragg grating (FBG) displacement meters. The results of the monitoring show that the position of the inner pit relative to the outer pit has a strong influence on the stability of the outer pit. The side on which the inner pit is closest to the outer pit wall is the most prone to instability and should thus be reinforced. Comparison and analysis of monitoring results obtained with optical fibers and CRLD bolts allow a potentially dangerous slip surface to be identified, indicating the value of using this type of collective monitoring in deep foundation pits.

1. Introduction

With the growing need to utilize underground spaces in urban areas, building structures have increasingly diverse comprehensive functionality. The installation of facilities such as elevator shafts, water collection wells, and mechanical equipment in the basement of building structures makes foundation pit design increasingly complicated. This has led to a move from single-level excavation pits to multilevel pits known as pit-in-pit foundations [1–3]. The wider peripheral area of the pit is termed the outer pit, and the deeper internal area is the inner pit. Thus, the outer pit and the inner pit form a complex foundation pit system. However, the research on pit-in-pit foundations is extremely scarce at home and abroad. As the influence of the inner pit on the outer pit cannot be ignored, monitoring and design of pit-in-pit foundations is clearly a research priority.

A pit-in-pit is a unique form in foundation engineering but it does have some excavation characteristics in common with conventional foundation pits. The stress-strain relationship in a conventional foundation pit changes with the excavation of the soil and is described well by the stress path method proposed by [4]. Model testing and numerical simulation have been adopted to study changes in the stress path of foundation soil under unloading conditions [5]. However, the structural form and earthwork construction of pit-in-pit foundations are different from those of a conventional foundation pit, and the postexcavation distribution of the stress field is more complicated. Pit-in-pit problems are not taken into consideration by the existing

design specifications of pit engineering, and the adoption of traditional foundation pit theory to design and construct pit-in-pit foundations fails to account for a number of factors, potentially resulting in major engineering accidents.

The current research into the pit-in-pit problem is limited to considering the construction method of the enclosure structure and analysis by numerical simulation. For example, the influence of excavating an inner pit in the outer pit has been analyzed on the basis of a large pit-in-pit foundation in Shanghai. Centrifuge model tests were conducted to investigate the deformation of a continuous underground wall for three different distances between the outer pit and inner pit, and numerical analysis was adopted to study the influence of outer pit width on the wall [6]. In another set of studies, changes in a pit-in-pit foundation were simulated with a PLAXIS numerical model, and the factors influencing the deflection of a wall by such a foundation were studied by orthogonal experimental design [7, 8]. However, few studies have concentrated on laboratory testing of pit-in-pit foundations, which would provide a more reliable reference for their design and construction in the field.

Due to a lack of research into stress and strain analysis in such systems, failures of pit-in-pit foundations have become increasingly frequent [9], occurring on a yearly basis in recent years. Outer pit failure in a braced excavation in soft soils usually leads to significant damage to adjacent structures. Thus, it is essential to assess the stability against outer pit failure for foundation pit design. On the other hand, because the effects of using a pit-in-pit configuration are often underestimated or not considered in calculations for the supporting structure, many designers have taken to overestimating the impact of using a pit-in-pit configuration, resulting in unnecessary engineering waste. Therefore, it is necessary to carry out in-depth research into the influence of a pit-in-pit configuration on the stability of the supporting structure and the deformation of the foundation pit so as to make the design of pit-in-pit foundations effective, economical, and reliable.

Foundations can be analyzed based on the field monitoring result, physical simulation, numerical simulation, and theoretical analysis. To explore the effects of subarea excavation on the deformation and stress of a metro foundation pit, the deep horizontal wall displacement, supporting axial force, and deformation of a metro foundation pit in Hangzhou city were measured [10]. A finite element analysis was performed on a soft embankment foundation improved by prefabricated vertical drains, and the equivalent permeability was used to conduct a plane strain analysis [11]. When the geometry of the project is relatively simple, mathematical and mechanical methods are most appropriate for calculating the stress field and strain field. However, these calculations become extremely involved when the geometry of the project is complex. The numerical method has to be simplified when conducting analysis for a complex engineering project, and the destruction theory of the soil body needs to be further improved. Compared with numerical simulation and theoretical analysis, physical simulation has the disadvantages of being time-consuming and labor-intensive, but tests on these models have dual applicability for the theory and practice of complex engineering projects. Therefore, in this study, a physical model was built in the laboratory, taking a typical pit-in-pit engineering project at Hefei Hengda Center in China as an example. Various tests were carried out to investigate the deformation of a pit-in-pit foundation under different loading and rainfall flow conditions. Compared with other monitoring methods for foundations, fiber optic monitoring method can achieve long-distance and large-area monitoring. CRLD bolt has a large deformation and high constant resistance function, and the anchor cable cannot be broken during the process of pit instability. Thus, these two methods are combined to monitor the stability characteristics of pit-in-pit, including stress and strain. This would be beneficial for early warning of pit instability, allowing timely remedial reinforcement to ensure the stability of the foundation pit. Based on the analysis of the instability caused in a typical foundation by the use of a pit-in-pit configuration, recommendations are made for the design and reinforcement of pit-in-pit foundations as a reference for geotechnical engineering designers.

2. Engineering Project Overview

2.1. Engineering Background. The engineering background for the laboratory test is the foundation pit project for Hefei Hengda Center, China, a schematic for which is shown in Figure 1. The foundation pit covers an area of 33,547.5 m^2 and is 194 m long, 184 m wide, and 8.5 m deep. In order to meet the requirements of the overlying building, an inner pit measuring 45 m long, 45 m wide, and 5.0 m deep is excavated in the foundation pit. The distances between the inner pit and outer pit are different on each side. Therefore, the supporting structure design for each side of the foundation pit should be modified depending on the potential for deformation of that side. It is therefore vital to investigate the stress and strain in this pit-in-pit foundation in detail.

2.2. Engineering Geological Conditions. The field investigations and in situ direct shear tests were carried out at the project site. The distribution and characteristics of soil layers at the foundation pit are shown in Table 1.

2.3. Hydrogeological Conditions. The project is located in the midlatitude zone and belongs to the subtropical monsoon humid climate. The climate is mild, and the annual average precipitation is about 1000 mm. The groundwater at the pit includes upper stagnant water, pore water, and bedrock fissure water, mainly supplied by precipitation and groundwater seepage. The upper stagnant water at the pit is affected by the terrain, topography, fill thickness, precipitation, and drainage from adjacent pits.

3. Experimental Studies

Real-time monitoring and early warning systems for foundation pits present a major challenge at present [10].

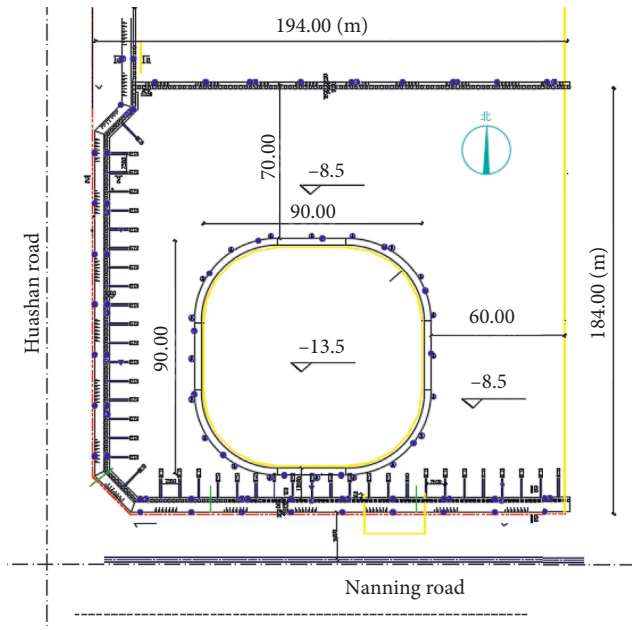

Figure 1: Plan view of the pit-in-pit foundation at Hefei Hengda Center in China.

Table 1: Distribution and characteristics of soil layers at the foundation pit.

Categories	Density ($kg \cdot m^{-3}$)	Elastic modulus (Mpa)	Poisson's ratio	Cohesive force (kPa)	Internal friction angle (°)	Depth range (m)
Clay	1900	25	0.29	55	19.4	0 to −1.81
Silty clay	1920	30	0.3	53	20.5	−1.81 to −10.94
Silty clay mixed with sand	1980	40	0.3	22	19.8	−10.94 to −21.71

This study adopts new technology and methods to monitor the stress and strain of a deep pit-in-pit foundation under the geologic conditions that pertain to Hefei Hengda Center and test whether these methods are capable of providing early warning of potential hazards.

3.1. Measurement Devices. Many factors, including the landform, surrounding geology, and weather conditions can affect foundation pit structures, causing engineering problems such as deformation, leakage, uneven settlement, and fracturing. Thus, it is critical to use appropriate sensor technologies to evaluate and predict the engineering stability of a foundation pit. Sensor monitoring technology can provide accurate and credible measurement data for engineering monitoring. The conventional sensor types include differential resistance sensors, resistive strain gauge sensors, inductive sensors, and vibrating-wire sensors, all of which have found several applications in engineering contexts [12–14]. However, the above-mentioned sensors have disadvantages, such as relatively low measurement accuracy, a small measurement range, or a lack of durability under large forces. Due to the advantages of a large monitoring range and the ability to provide early warnings, BOTDA (Brillouin optical time-domain analyzer) optical fibers and CRLD (constant resistance and large deformation) bolts are adopted by this study to monitor the stress and strain of a deep pit-in-pit, assisted by soil pressure cells and extensometer monitoring. Coupling these monitoring devices and methods enables the effective measurement of internal stress and strain at the foundation pit.

3.1.1. Principles of BOTDA Optical Fiber Monitoring. Due to the many advantages of Brillouin distributed optical fiber sensors, which include small size, ease of installation, and rapid data transmission, they have been widely applied for monitoring geotechnical engineering stability in recent decades [15–18]. Strain-sensing optical fibers can be installed over several and even tens of kilometres. Sampling points can be placed at intervals of tens of centimetres to several meters along the fiber so as to monitor the strain condition continuously. This allows the global strain behavior of whole structures to be measured without being affected by local stress/strain concentrations.

The BOTDA technique is based on stimulated Brillouin backscattering [19, 20]. Two laser sources, a pulsed laser and continuous laser, are introduced from the two ends of the optic fiber (Figure 2). When the frequency difference between the two lasers is equal to the Brillouin frequency shift,

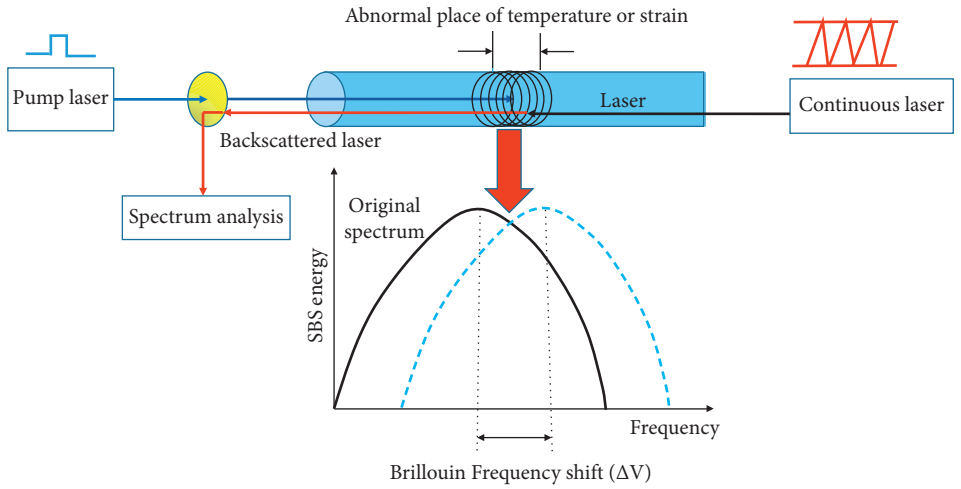

Figure 2: Operating principle of BOTDA [21].

Brillouin backscattering will be stimulated and energy transfer will occur between the two lasers, as shown in Figure 2.

The Brillouin frequency shift ν_B changes in proportion to the variation in strain or temperature. These linear relationships can be expressed as

$$\begin{aligned} \nu_B(T_0, \varepsilon) &= C_\varepsilon(\varepsilon - \varepsilon_0) + \nu_{B0}(T_0, \varepsilon_0), \\ \nu_B(T, \varepsilon_0) &= C_T(T - T_0) + \nu_{B0}(T_0, \varepsilon_0), \end{aligned} \tag{1}$$

where C_ε and C_T are the strain and temperature coefficients, respectively, and T_0 and ε_0 are the strain and temperature, respectively, that correspond to a reference Brillouin frequency ν_{B0}.

The propagation time of light pulses transmitted in the fiber is measured and subjected to time-domain analysis to derive spatial information about the fiber and the continuous temperature and strain distributions along it. An optical inclinometer tube comprises the optical fiber and a tube, with optical fiber being distributed symmetrically on both sides of the tube. The horizontal strain at the tube can be obtained by integrating the strain measured by the optical fiber on either side of the tube. A strain/loss analyzer (NBX-6050A fiber strain demodulator) based on the BOTDA technique is used for continuous strain distribution measurement with an optical fiber sensor (Figure 3).

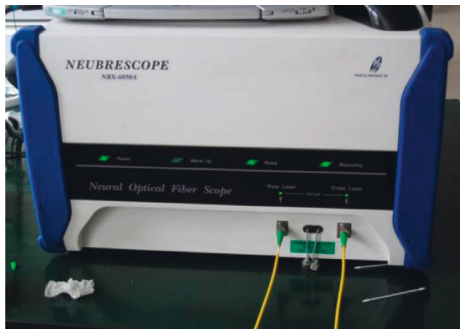

Figure 3: NBX-6050A fiber strain demodulator.

3.1.2. Principles of CRLD Bolt Monitoring. A novel energy-absorbing bolt, known as a constant resistance and large deformation (CRLD) bolt [22–26], is adopted for this monitoring project. The bolt has a compound structure, consisting of a cone-like piston that slides inside an elastically-deformable sleeve pipe (Figure 4). The frictional resistance generated by the sliding of the cone body relative to the internal surface of the sleeve pipe can be mathematically formulated, as it is dependent on the elastic properties of the sleeve pipe, the geometry of the cone, and the frictional properties of the sliding interface and independent of the external loads under static loading conditions [22]. The special structure of the CRLD bolt means that the diameter of the constant resistance structure increases under extension. This effect gives the bolt the properties of a large degree of elongation, strong energy absorption, and high resistance.

A miniature constant-resistance monitoring bolt suitable for laboratory model experiments was designed based on the CRLD bolt researched and developed by [22]. The CRLD bolt consists of a constant resistance body, a constant resistance sleeve (with an inner diameter slightly smaller than the diameter of the large end of the constant resistance body), a rod, a tray (which transmits the deformation of the rock mass to the constant resistance sleeve), and a fastening nut. The structure of the CRLD bolt and miniature bolt are shown in Figure 5(a).

The core component of the CRLD bolt is a constant resistance device in which the material strength of the constant resistance sleeve is lower than that of the constant resistance body. This unique design provides constant resistance as the body slides in the constant resistance sleeve. The lower strength causes friction, resulting in the resistance reduction characteristics and constant resistance performance of the CRLD bolt. A miniature version of the constant resistance device shown in Figure 5(b) was prepared for convenience in testing.

One side of each CRLD bolt is fixed inside the foundation pit, and the other is anchored in the inner wall of the

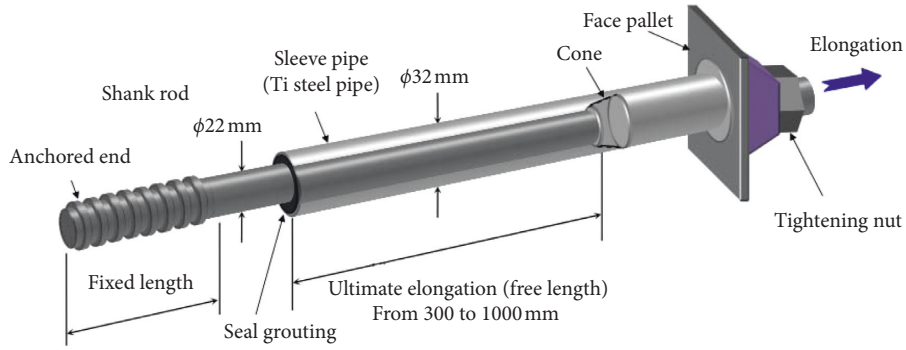

Figure 4: Three-dimensional schematic of a CRLD bolt.

(a) (b)

Figure 5: Assembly diagram of CRLD monitoring device. (a) Diagram of a miniature constant resistance and large deformation bolt. (b) Views of a miniature constant resistance device, large deformation bolt, and data collector.

foundation pit. Dynamometers are set under the fixed part to acquire data on change in the internal force in the bolts, which are equivalent to the force at the position around the bolts. Professor He developed the principle by which CRLD bolts provide early warning: a sudden drop in the rising internal force of the bolts indicates that a sliding surface has begun to penetrate. CRLD bolts can thus be applied for monitoring the stability of foundation pits, providing forewarning of deep foundation pit instability.

3.1.3. Fiber Grating Displacement Meters and Soil Pressure Cells. FBG (fiber Bragg grating) sensors can perform a direct transformation of a sensed parameter into a shift in wavelength, which can then be converted into power or current change through a demodulator. FBG sensors, including soil pressure gauges and displacement meters, have been used in strain and temperature sensor applications [27–29].

FBG soil pressure gauges are effective for monitoring the variation in lithostatic pressure inside the structure. The FBG sensing element is embedded in the measured structure, and when the pressure inside the structure changes, the periodic structure of the FBG changes because the pressure on the sensor causes a change in the wavelength output from the soil pressure cell. The output wavelength can be correlated to the soil pressure in the structure, and the temperature of the buried point can also be measured simultaneously.

FBG displacement meters can be used to measure the degree of displacement during the opening and closing of expansion joints (or cracks) in a structure. An FBG displacement meter is mounted at both ends of the gap. When the degree of opening or closing of the gap changes, the periodic structure of the FBG also changes, causing changes in the output wavelength of the sensors. The output wavelength is fed to an FBG demodulator, which transforms these data to obtain the variation in relative displacement of the expansion joints or cracks. Again, the temperature at the buried point is measured simultaneously.

3.2. Physical Model Tests

3.2.1. Test Design. This experiment uses physical modelling to simulate the deformation of a pit-in-pit foundation under loading and rainfall flow conditions, taking Hefei Hengda Center as its prototype. As the ratio of the pit length to pit depth is relatively large, qualitative assessment of the stress and strain of the pit-in-pit foundation is facilitated by setting a geometric similarity ratio. The geometric scale factor for the length and width, which is defined as the ratio of that dimension in the real foundation to that in the physical model, is determined to be 200, while the geometric scale factor for the height is 10. The size of the experimental model is thus set at 1.77 m × 1.72 m × 1.2 m, in which the outer pit size is 0.97 m × 0.92 m × 0.85 m, the inner pit size is 0.45 m × 0.45 m × 0.5 m, and the width of soil body outside each side of the foundation pit is 0.4 m. The distances between the inner and outer pits are different on each side. They are closest on side No. 1, where they are 120 mm apart. The distances on sides No. 2, No. 3 and No. 4, which are numbered from No. 1 in a clockwise direction, are 200 mm, 350 mm and 300 mm, respectively. A three-dimensional top view with the dimensions marked is shown in Figure 6. Original field samples of clay and silty clay were transported

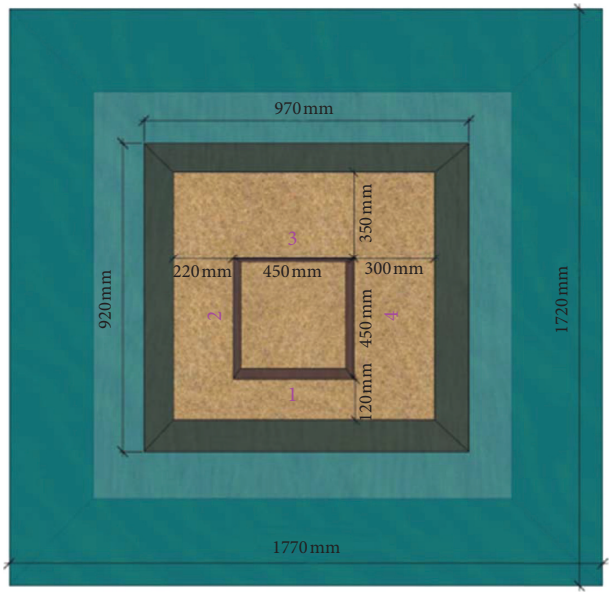

Figure 6: Three-dimensional top view of the foundation pit.

to the laboratory to fill the foundation pit model in accordance with the thickness of soil layers in the C block of the Hengda Center, Hefei.

The primary aim of this experiment is to simulate the process by which a pit-in-pit foundation deforms under loading and rainfall. Therefore, the configuration in which the optical fiber is laid is an important consideration. Figure 7 shows the setup for the optical inclinometer tubes and fiber schematically in three dimensions (the x direction is the direction of horizontal deformation, and the z direction is the direction of settlement of the foundation pit). The optical inclinometer tubes are used to monitor the horizontal strain in the x direction and are set up in two squares. The tubes in the outer square (X1) have a monitoring length of 135 cm and are named X11–X18 from side No. 1 to side No. 4, with two optical inclinometer tubes set on each side of the outer pit. Those in the inner square (X2), which have a monitoring length of 50 cm, are named X21–X24 from side No. 1 to side No. 4, with one optical inclinometer tube set up on each side of the inner pit. The optical fiber is used to monitor the settlement strain in the z direction. It is also set up in two squares in the same configuration as the optical inclinometer tubes, with the outer square (Z1) consisting of eight lengths of fiber referred to as Z11–Z18 and the inner square (Z2) consisting of lengths of fiber labelled Z21–Z28. The monitoring lengths are also the same as for the optical inclinometer tubes.

Point fixation (PF) installation of the optical fiber results in a uniform strain distribution between any two bonding points, which are at intervals of 20 cm. The two optical inclinometer tubes on each side of the outer pit are symmetrically distributed at a distance of 500 mm from each other, and the optical inclinometer tubes for the inner pit are set at the midpoint of each of its sides. The optical fibers for the outer pit are set at 25%, 50%, and 75% along each side of the outer pit, as are those along each side of the inner pit.

The CRLD bolts are arranged in two squares at a height of 0.35 m within the pit. Each inner side of the inner pit is anchored with two CRLD bolts, which are named B21–B28 from side No. 1 to side No. 4. Each inner side of the outer pit is anchored at a height of 1 m with three CRLD bolts, which are named B11–B112 from side No. 1 to side No. 4. A total of 20 CRLD bolts are thus installed in the foundation pit. Fiber grating displacement meters and soil pressure cells are adopted to monitor the horizontal displacement and soil pressure inside the foundation pit to verify and assist the other monitoring devices. The soil pressure cells are buried in two layers on each side of the outer pit at a height of 0.4 m and 0.9 m, respectively, and the displacement meters are arranged in a single square at a height of 0.7 in the outer pit, one on each side. The three-dimensional arrangement of the CRLD bolts and FBG devices is shown in Figure 8.

Thus, a 1.77 m × 1.72 m × 1.2 m pit-in-pit foundation model was constructed and reinforced with the various sensors laid at positions dictated by the experimental design, and the fibers were welded to form a distributed monitoring network (Figure 9).

Tests were carried out with the foundation pit relatively stable. As the scale of the model is small, the inner template of the foundation pit was left in place with a penetration depth of 15 cm to act as an antislide pile, reinforcing the foundation pit. Dynamometers were connected with the stress demodulators to monitor variation in the internal stress of the pit, and the fiber was connected with an NBX-6050A type fiber optic strain demodulation instrument to monitor the deformation inside the pit. The fiber grating displacement meters and soil pressure cells were connected to the distributed safety monitoring data acquisition system to enable measurement (Figure 10).

Among the many factors that affect the stability of a deep foundation pit, loading and rainfall are relatively important. Therefore, the experiment was divided into two parts, simulating the deformation of the foundation pit under different loads and under different rainfall conditions. As there is a high density of buildings around the C block area of Hefei Hengda Center, the first part primarily simulated the influence of surrounding buildings on the deformation of the foundation pit. Wooden boards were laid on the four sides of the foundation pit so that loads could be uniformly distributed in the soil body. Tests were conducted with loads of 50 kg, 100 kg, and 150 kg on each side. Deformation was measured when the soil mass became stable. The second part simulated the influence of rainfall on the deformation of the pit under constant loading. A rainfall time of 5.2 h is required to reach the local maximum measured at Hengda Center, Hefei, with indoor rainfall equipment (Section 3.2.3). Therefore, the model was exposed to 5.2 h of daily rainfall on three consecutive days. Monitoring data were obtained each day to compare and analyze the influence of rainfall on the internal stress and strain of the foundation pit.

3.2.2. Tests of the Pit-in-Pit Foundation under Different Loads. The deformation of the optical fiber was first

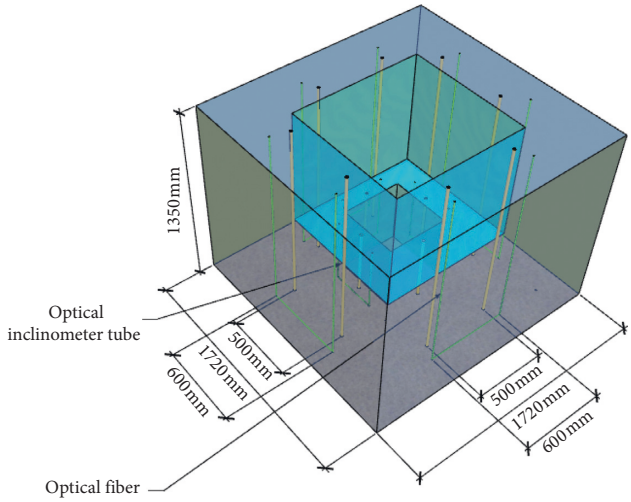

Figure 7: Three-dimensional arrangement of optical inclinometer tubes and fiber.

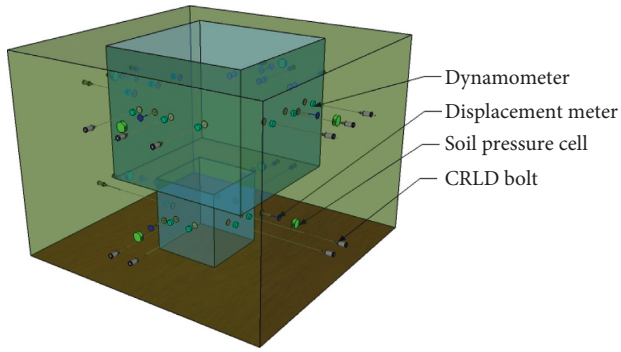

Figure 8: Three-dimensional arrangement of CRLD bolts and FBG sensors.

(a) (b)

Figure 9: The layout of monitoring devices in the experiment.

measured before loading. Next, experiments were run with loads of 50 kg, 100 kg, and 150 kg on the four sides of the foundation pit (Figure 11). After the pit stabilized, the deformation of each optical fiber, the tension value on the bolt, and the values captured by the displacement meters and soil pressure cells were recorded.

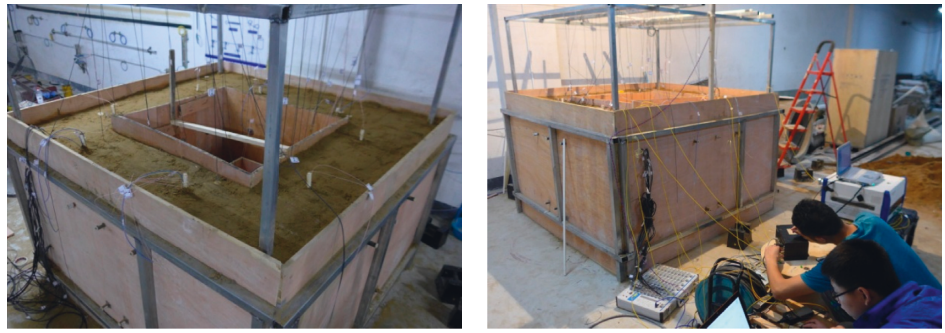

(a) (b)

Figure 10: The connection between (a) monitoring equipment and (b) data collectors.

3.2.3. Tests of the Pit-in-Pit Foundation under Different Rainfall Conditions. The indoor rainfall equipment includes flexible conduit, sprinkler, electromotor, and water storage tank. The outlet end of the flexible conduit is connected with the water storage tank, and a flowmeter with a control valve is fixed on the flexible conduit to control the rainfall magnitude. The rainfall time required to reach the local maximum for Hengda Center, Hefei, with indoor rainfall equipment can be determined using the following formula:

$$t = \frac{ps}{v}, \tag{2}$$

where t is rainfall time/h; p is local daily maximum rainfall/mm; s is rainfall area/m^2; and v is the hourly rainfall attainable with indoor rainfall equipment/(L/h). The local daily maximum rainfall p is 104 mm, the hourly rainfall v is 60 L, and the area of the foundation pit model s is 3 m^2. Therefore, the required rainfall time t is calculated to be approximately 5.2 h. Therefore, the model was subjected to 5.2 h of daily rainfall on three consecutive days. A slight displacement of the antislide pile could be seen as the rainfall continued, and a relative displacement occurred between the constant resistance body and constant resistance sleeve of the bolts (Figure 12). The strain in each optical fiber, the internal force of the bolts, and the values from the displacement meters and soil pressure cells under different rainfall conditions were measured. Then, the strain and stress in the foundation pit on different days were compared and analyzed. The experimental setup is shown in Figure 13.

4. Experimental Results and Discussion

Strain-sensing optical fiber cooperatively deforms with the soil mass. In the data derived from it, the positive direction indicates tension and the negative direction indicates compression. The parameters of the optical fiber strain analyzer were set to the values shown in Table 2 according to the laying method of the optical fiber and the characteristics of the pit. Each optical inclinometer tube and fiber data point is the difference from the initial value, i.e. the strain change value, and these are combined to produce deformation profiles for the foundation pit.

4.1. Analysis of Horizontal Deformation of the Pit-in-Pit Foundation. Tubes X11–X18 gave horizontal deformation curves for the outer pit, and X21–X28 gave horizontal deformation curves for the inner pit.

4.1.1. Horizontal Deformation of the Outer Pit. Excavating a pit-in-pit foundation is equivalent to changing the upper boundary of a semi-infinite body so that the in situ stress field is redistributed and deformation is generated in the corresponding stratum. Comparison of monitoring results acquired by the optical inclinometer tubes (Figure 14) indicates that the horizontal deformation of each side, especially for side No. 1, increased with increasing load. The maximum deformation, a strain value of 1095 $\mu\varepsilon$, was recorded between a depth of 0.3 m and 0.35 m at the X12 inclinometer tube. The horizontal strain of side No. 3 was relatively small compared to that of the other sides. This was mainly because the distance between the outer and inner pits was smallest on side No. 1 and greatest on side No. 3. Therefore, the supportive force provided by the lower soil on side No. 1 was relatively small compared to that on the other sides, causing it to deform more. In the rainfall experiments, the peak deformation increment of each side was highest after the first rainfall, reaching a maximum of 415 $\mu\varepsilon$. On subsequent days, the deformation of each side increased gradually. However, the deformation increment (the incremental value of the day compared with the previous day) gradually decreased, and the strain increments on each side after the second and third days of rainfall decreased in turn compared with that of the previous day. This can be attributed to the fact that the soil body was initially in a loose granular state with high porosity and compressibility. Under the action of rainfall, soil particles were subjected to erosion by rainwater, and the flow of pore water drove deformation in the soil body. The soil body then gradually became saturated, causing the deformation of the pit to decrease gradually. The horizontal deformation suddenly increased at a depth of 0.3 m at the X12 optical inclinometer tube, possibly indicating the existence of a potential slip surface; this should be considered in follow-up analysis. At the end of the first rainfall, the soil body began to consolidate and settle, becoming more compact and less compressible.

(a) (b)

Figure 11: Pit-in-pit tests under different loading conditions.

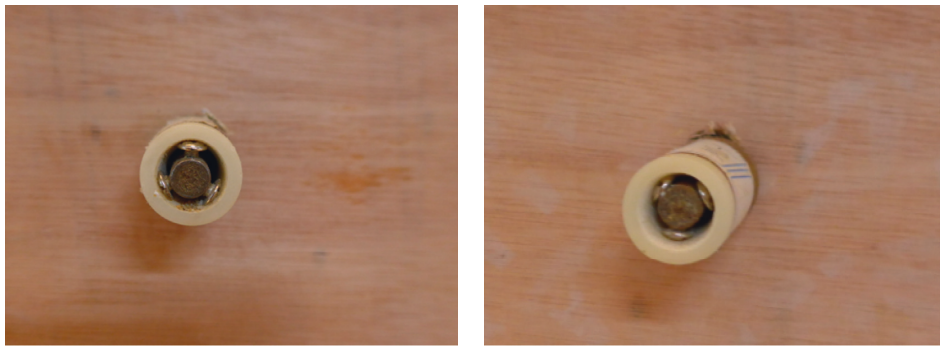

(a) (b)

Figure 12: A relative displacement between (a) the constant resistance body and (b) sleeve of bolt B12.

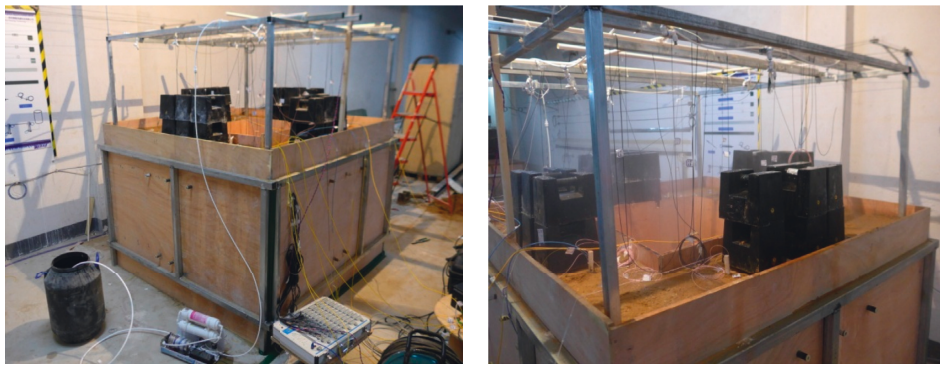

(a) (b)

Figure 13: Pit-in-pit tests under different rainfall conditions.

Table 2: Parameter settings for the fiber strain analyzer.

Measuring range (m)	Sampling interval (m)	Average number of times (time)	Starting frequency (GHz)	Scanning interval (MHz)	Termination frequency (GHz)
100	0.05	2^{16}	10.700	5	12.195

Thus, the effects of the second and third rainfall on the horizontal deformation were smaller, indicating that the whole soil body was in a relatively stable state.

4.1.2. Horizontal Deformation of the Inner Pit. Due to its smaller span and stronger bending resistance, the inner pit had smaller horizontal strains than the outer pit (Figure 15).

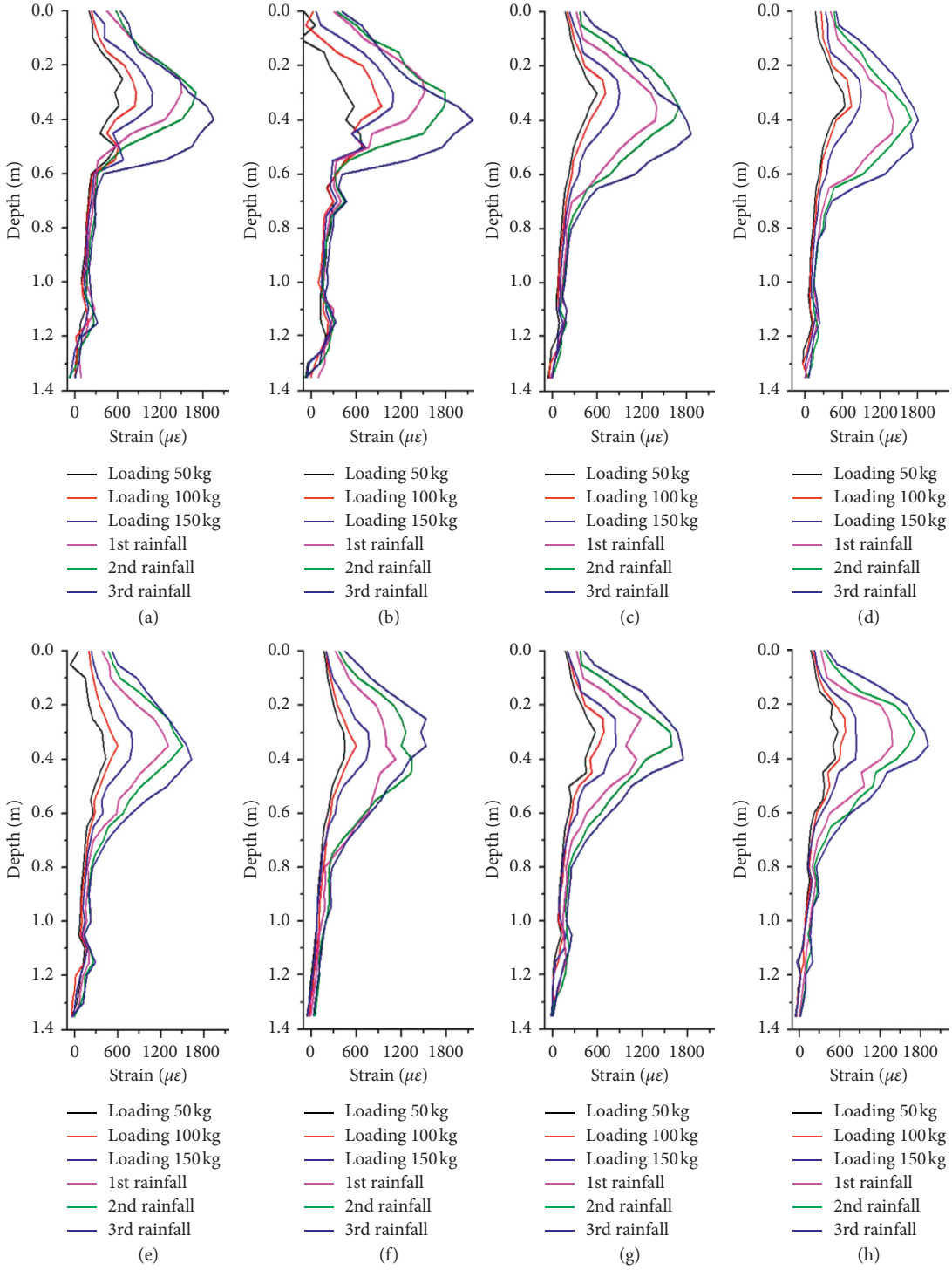

Figure 14: Horizontal strain curves measured by optical inclinometer tubes for the outer pit under different conditions: (a) X11 tube; (b) X12 tube; (c) X13 tube; (d) X14 tube; (e) X15 tube; (f) X16 tube; (g) X17 tube; (h) X18 tube.

However, due to the effects of external force, the self-weight of the soil body and the different distances between the inner and outer pit on each side, the support force provided by the soil body to the inner pit also differed significantly between sides, and the horizontal strain values likewise differed. The horizontal strain monitoring around the inner pit shows that the part of the inner pit wall with the maximum horizontal deformation was inclined to the middle and lower parts. The maximum horizontal deformation of the inner pit occurred in side No. 1, reaching a strain of 1400 $\mu\varepsilon$, and the maximum strain values of the other three sides under the same working condition were 1140 $\mu\varepsilon$, 860 $\mu\varepsilon$, and 994 $\mu\varepsilon$, respectively. As there was no loading on the inner pit, the deformation of the upper part

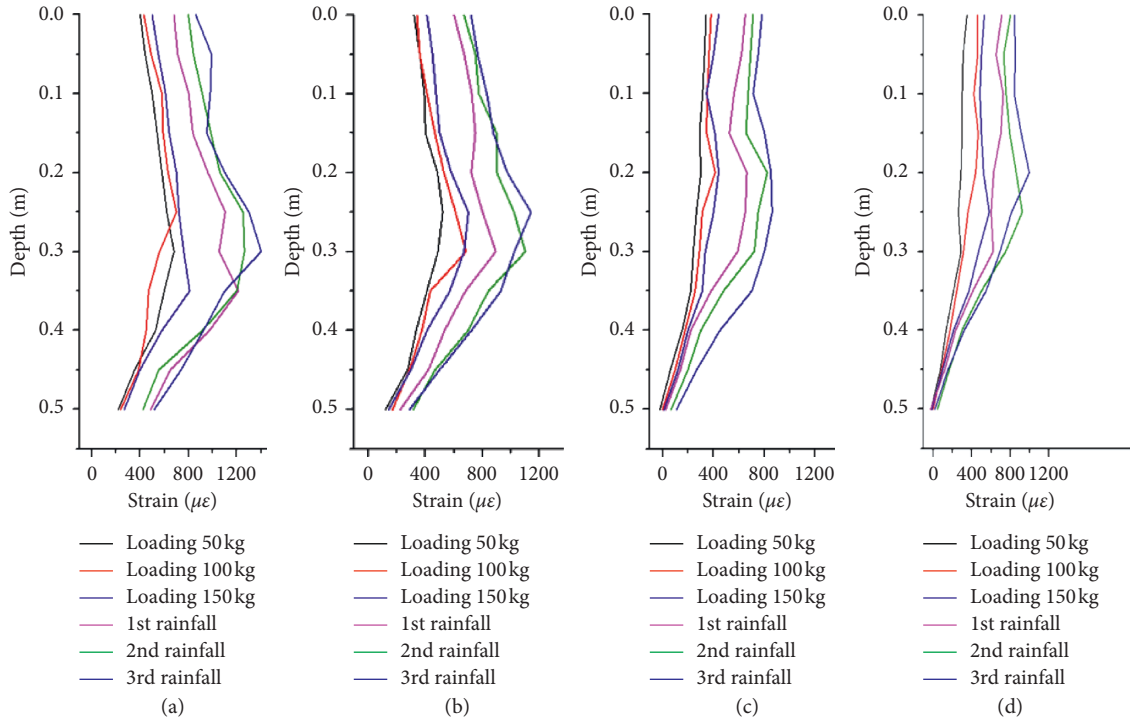

Figure 15: Horizontal strain curves measured by optical inclinometer tubes for the inner pit under different conditions: (a) X21 tube; (b) X22 tube; (c) X23 tube; (d) X24 tube.

was not restricted, and the horizontal deformation in the upper part was larger than in other parts.

4.2. Analysis of Settlement of the Pit-in-Pit Foundation. Fibers Z11–Z18 gave the vertical settlement curves for the outer pit, and Z11–Z18 gave the vertical settlement curves for the inner pit.

4.2.1. Settlement of the Outer Pit. The antislide piles in the outer pit are not only squeezed by the soil body behind the pile but are also bound by the soil body of the inner pit. Therefore, when the distances between the excavation location of the inner pit and outer pit are not the same on all sides, the strain field and stress field of a pit-in-pit foundation cannot be symmetrical. Instead, there will be obvious differences in the horizontal displacement of the antislide piles on each side, and the horizontal displacement of the antislide piles will largely determine the scope and size of surface settlement [7].

The vertical settlement on each side of the pit system was similar under different loads (see Figure 16). The vertical settlement on side No. 1 was relatively large because the horizontal strain of side No. 1 was larger than that of the other sides. In the rainfall experiments, the settlement increment reached a maximum after the first rainfall, and the increment was basically stable after the second rainfall. The settlement curves with depth in the pit presented a sawtooth shape. This is possibly due to the effect of rainwater infiltration, as the small particles in the rock mass caught up in pore water flow impact the optical fiber, resulting in a local strain mutation of the fiber. However, as the impact force is small, it has little effect on the overall strain trend of the optical fiber.

4.2.2. Settlement of the Inner Pit. Adjacent optical fibers on the same side have roughly the same trend in Figure 17. The settlement on each side of the inner pit is similar under loading and under rainfall but with a larger settlement increment under rainfall. Thus, rainfall had a greater effect on the settlement of the inner pit than did loading, mainly due to the scouring effect of rainfall.

4.3. Stress Analysis under Loading and Rainfall. Bolts B21–B28 gave stress curves for the inner pit, and B11–B112 gave stress curves for the outer pit. The internal force curves of the CRLD bolts (Figure 18) show that stress in the foundation pit increased smoothly with increased loading. However, there was a clear growth in stress after rainfall due to the hydrodynamic force driving the soil body to press against the antislide pile. The internal force of the bolts in side No. 1 was the largest. This is because the horizontal deformation of side No. 1 was greater than that of the other sides, causing the antislide pile on side No. 1 to be squeezed by the soil behind it and because the binding force provided by the inner pit soil body was relatively small. In general, the internal force of the bolts in the outer pit was larger than that of the bolts in the inner pit. The internal forces of bolts B12 and B13 in side No. 1 increased after rainfall for the first two days but decreased after the third rainfall. The rate of decrease was greatest for bolt B13, reaching 38.5%.

According to the internal force monitoring criteria of CRLD bolts, when there is a sudden drop in the internal

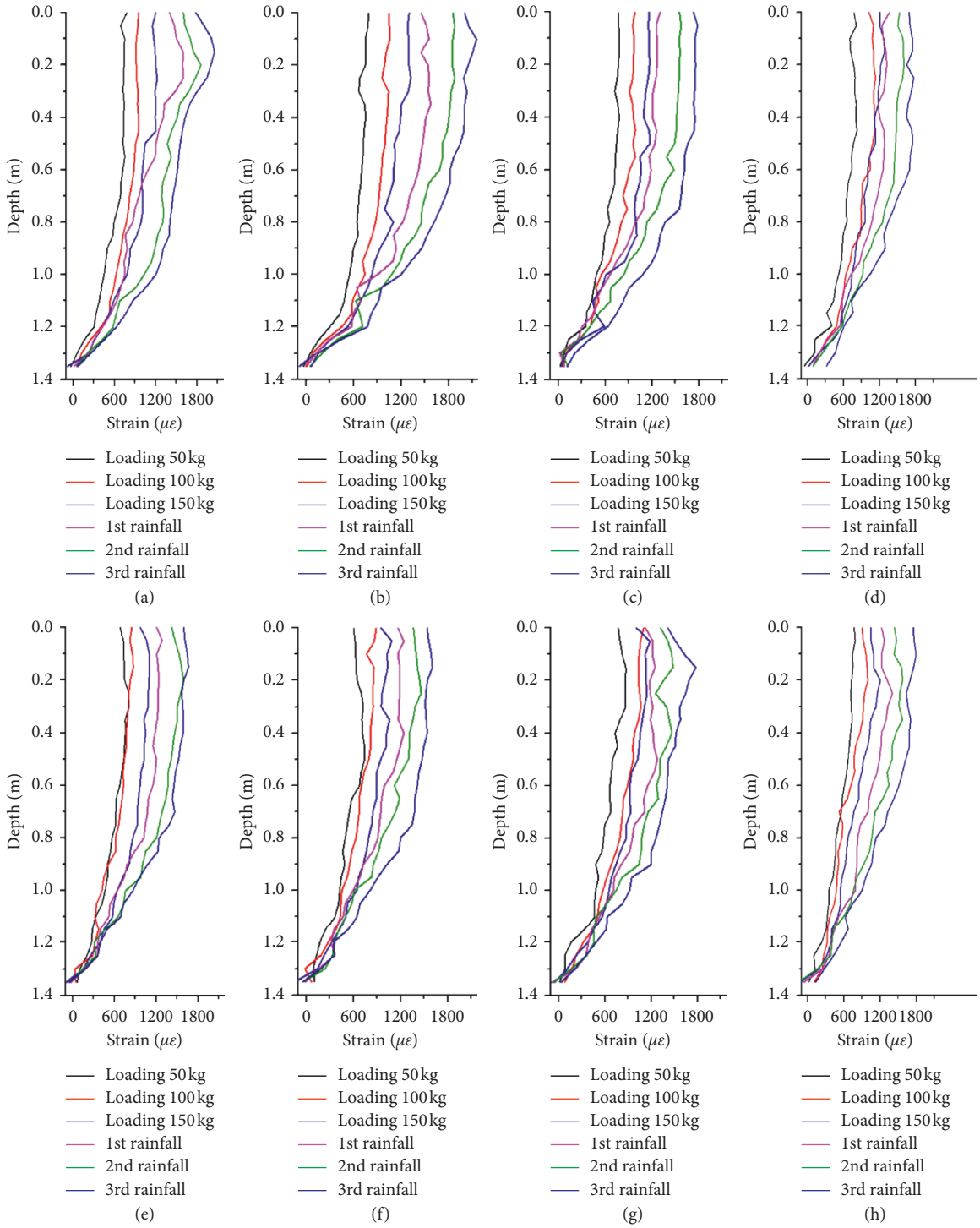

Figure 16: Settlement curves measured by optical fiber for the outer pit under different conditions: (a) Z11 optical fiber; (b) Z12 optical fiber; (c) Z13 optical fiber; (d) Z14 optical fiber; (e) Z15 optical fiber; (f) Z16 optical fiber; (g) Z17 optical fiber; (h) Z18 optical fiber.

force of bolts, the characteristics of the foundation show partial slippage or overall slippage, but the sliding bodies are not completely disintegrated from the foundation. The time at which the sliding bodies are completely disintegrated lags behind the time corresponding to the sudden drop in the internal force. Therefore, there is a certain span of time during which people can evacuate safely or reinforce the foundation in advance. The internal force monitoring curve of CRLD bolts indicates that the area around bolt B13 was a potential sliding surface, though it was not yet penetrating. The stress monitored by the other bolts still increased constantly. Therefore, these data combined with the deformation data measured by optical fiber indicate that side No. 1 of the outer pit, especially near side No. 2, was the most unstable part of the pit system. This can be attributed to the distance between the outer and inner pits on this side. The

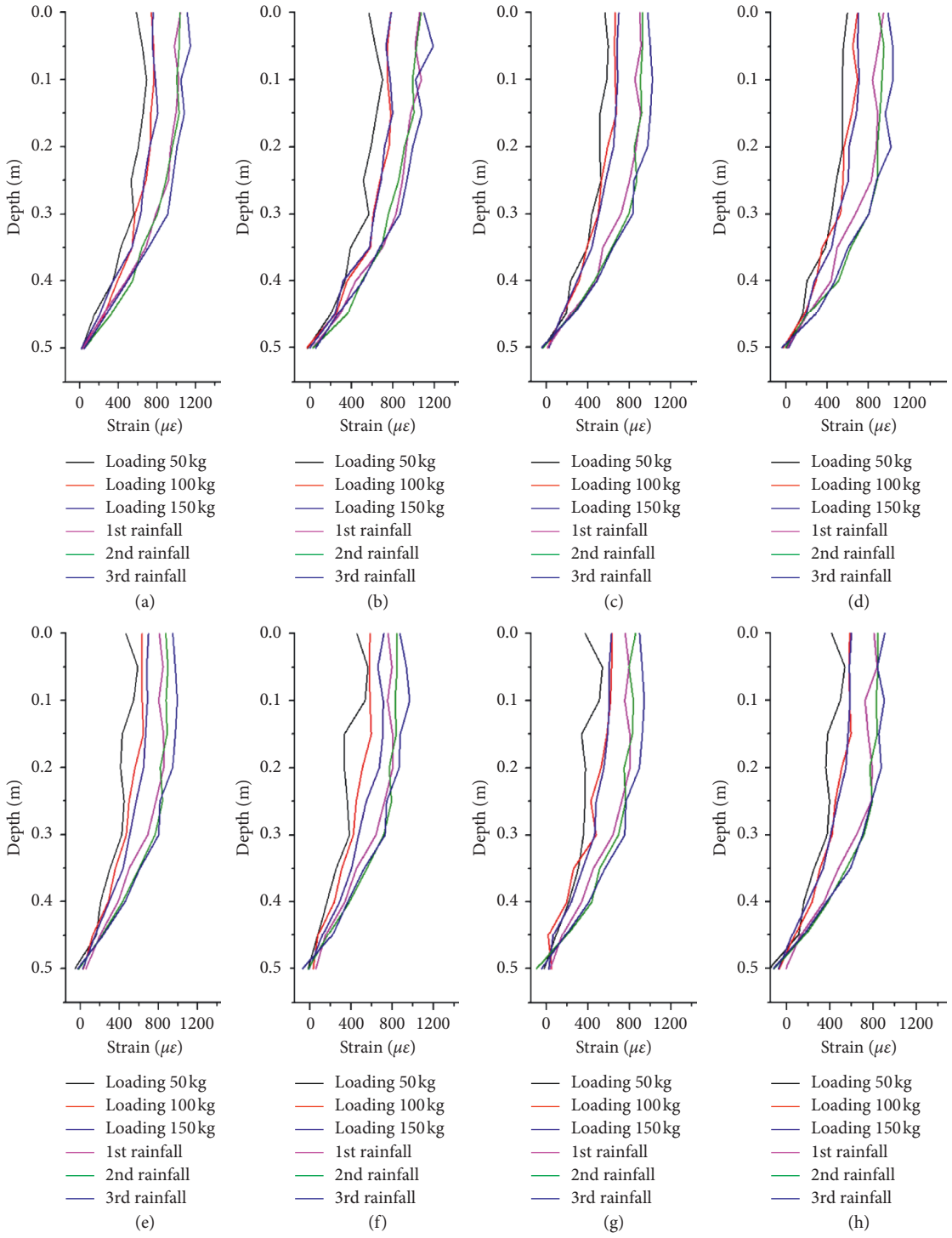

Figure 17: Settlement curves measured by optical fiber for the inner pit under different conditions: (a) Z21 optical fiber (b) Z22 optical fiber; (c) Z23 optical fiber; (d) Z24 optical fiber; (e) Z25 optical fiber; (f) Z26 optical fiber; (g) Z27 optical fiber; (i) Z28 optical fiber.

smaller the distance between the outer and inner pits, the less the binding force exerted on the outer pit.

4.4. Analysis of Monitoring Results Obtained by FBG Displacement Meters and Soil Pressure Cells. D1–D4 gave displacement curves for the outer pit, P11–P14 gave soil pressure curves for the upper part of the soil body, and P21–P24 gave soil pressure curves for the lower part of the soil body.

The monitoring curves in Figure 19 show that the data from the FBG displacement meters followed the same trends as those from the optical inclinometer tubes. The horizontal displacement value for side No. 1 (measured by D1) was larger than that for the other sides, which is in agreement with the results from the fiber and CRLD bolt monitoring. As shown in Figure 20, a higher pressure value was obtained for the upper soil body than

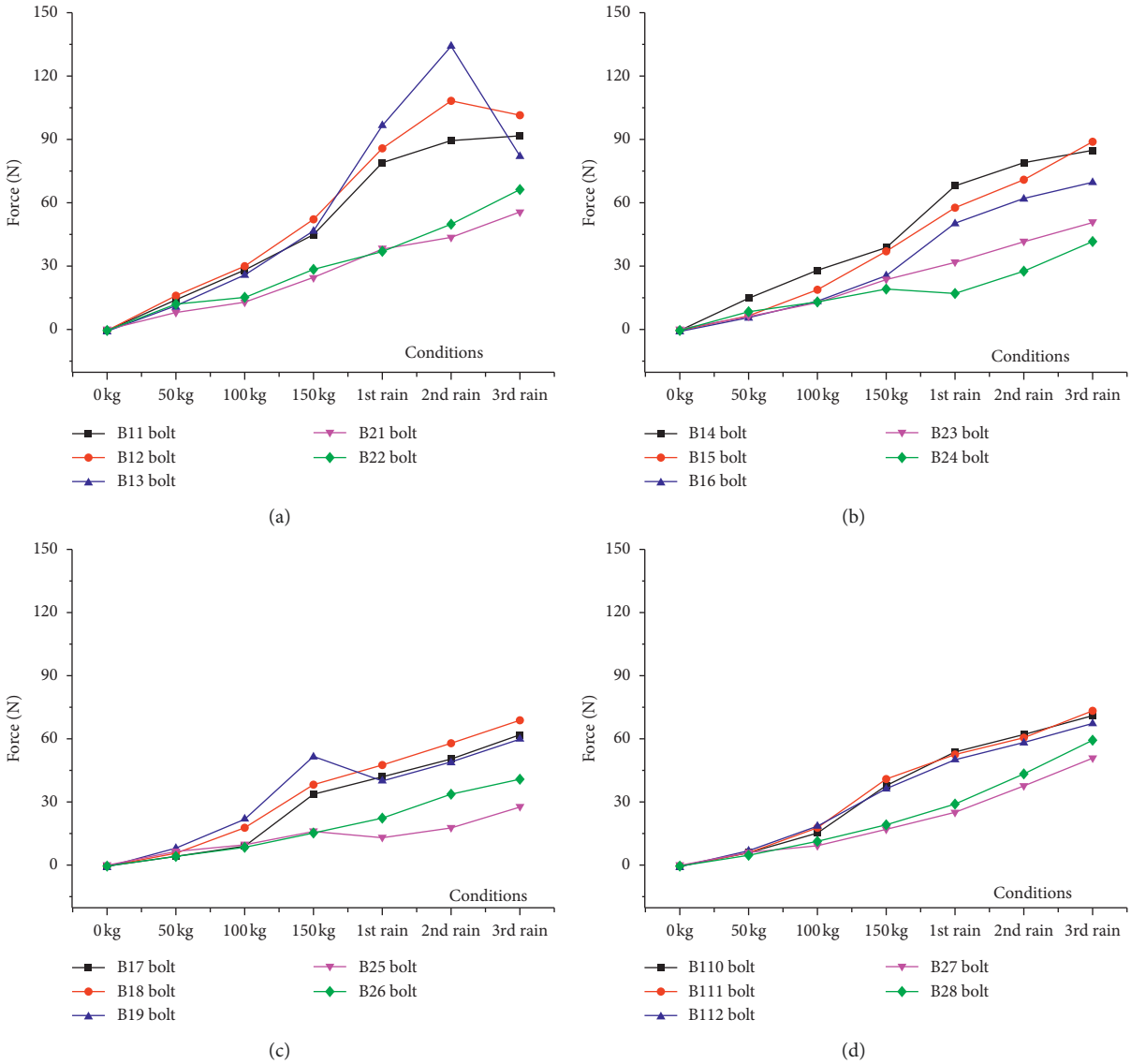

Figure 18: Internal force monitoring curves of CRLD bolts under different conditions: (a) internal force of bolts in side No. 1; (b) internal force of bolts in side No. 2; (c) internal force of bolts in side No. 3; (d) internal force of bolts in side No. 4.

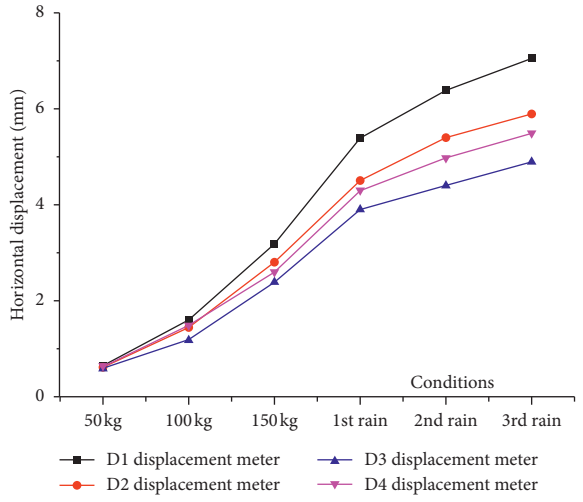

Figure 19: Monitoring curves from FBG displacement meters under different conditions.

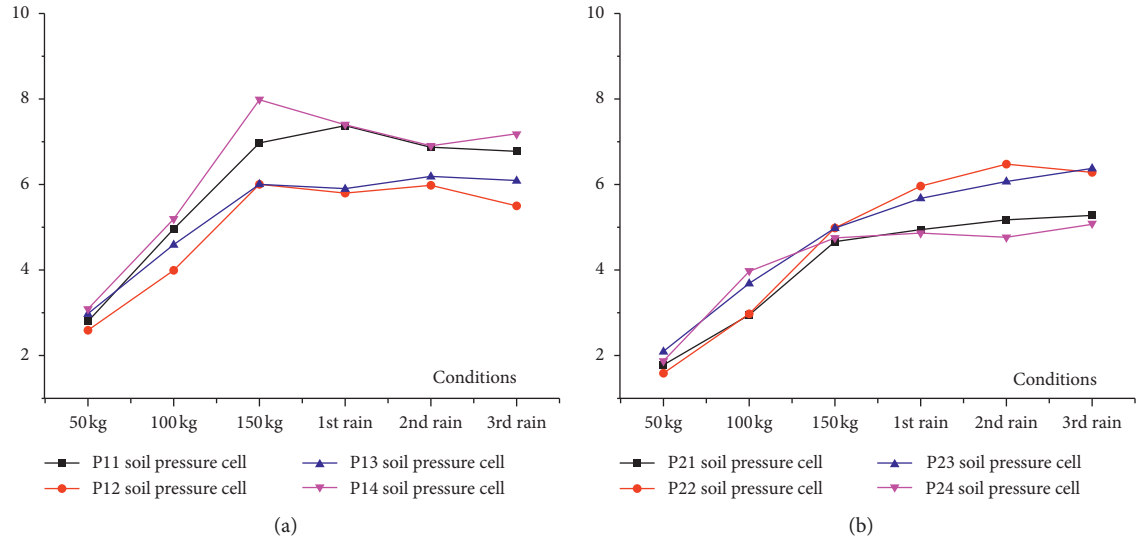

Figure 20: Monitoring curves from FBG soil pressure cells under different conditions: (a) soil pressure curves for the upper part; (b) soil pressure curves for the lower part.

the lower soil body. Pressure in the upper soil gradually decreased and reached a relatively steady state with continuous rainfall. The measured pressure value of the lower soil continued to increase slightly with more rainfall, mainly due to small particles from the upper soil being introduced into the lower part of the pit under rainfall-induced erosion.

5. Conclusion

The physical model of pit-in-pit was employed to qualitatively investigate the effects of excavating an inner pit on the stress and strain field of an outer pit, with Hefei Hengda Center as the prototype. Optical fiber and CRLD bolts were adopted to monitor the stability of the pit-in-pit foundation. The following conclusions were obtained:

(1) The position of the inner pit relative to the outer pit has a major effect on the stability of the outer pit. The sides on which the margins of inner and outer pits are closest are the most prone to instability and should therefore be emphatically reinforced. The sides where the two pits are furthest apart are relatively stable.

(2) Rainfall is an important cause of foundation pit instability, especially for pit-in-pit configurations. Under the action of rainfall, soil particles are eroded by the rainwater, and pore water flow drives deformation in the soil body. Thus, drainage of pit-in-pit foundations should be paid more attention.

(3) Internal force of bolts and strain inside the foundation pit can be considered as the monitoring factors of pit instability. Taking these two factors comprehensively into account enables the realization of early warning of pit instability, allowing timely remedial reinforcement to ensure the stability of the foundation pit.

(4) The comparison and analysis of monitoring results measured by optical fiber and CRLD bolts allow dangerous slip surfaces to be easily identified. Therefore, these are effective methods for monitoring pit stability and can be applied to collectively monitor deep foundation pits.

Data Availability

The data are all available and has been explained in this article, and the readers can access the data supporting the conclusions of the study.

Conflicts of Interest

The authors declare that they have no conflicts of interest.

Acknowledgments

This work was supported by the Key Research and Development Project of Zhejiang Province (Grant No: 2019C03104).

References

[1] F. Cai, K. Ugai, and T. Hagiwara, "Base stability of circular excavations in soft clay," *Journal of Geotechnical and Geoenvironmental Engineering*, vol. 128, no. 8, pp. 702–706, 2002.

[2] W. C. Pan, "The inner retaining wall and relevant influence to outer retaining wall," in *Ninth National Symposium on Foundation Treatment*, pp. 397–399, Zhejiang University Press, Hangzhou, China, 2006.

[3] M. L. Shen, S. M. Liao, X. H. Zhou et al., "Parametric analysis on stress field of pit in pit excavation," *Chinese Journal of Geotechnical Engineering*, vol. 32, no. 1, pp. 187–191, 2010.

[4] T. W. Lambe, "Stress path method," *Journal of the Soil Mechanics and Foundations Division*, vol. 93, no. SM6, pp. 268–277, 1967.

[5] Z. K. Hua and C. K. Shen, "Lateral earth pressure on retaining structure with anchor plates," *Journal of Geotechnical Engineering*, vol. 113, no. 3, pp. 189–201, 1987.

[6] J. S. Huo, J. Chen, Q. M. Gong, and S. H. Zhou, "Study on the deformation of retaining structure of pit-in-pit excavation," *Advanced Materials Research*, vol. 243–249, no. 3-4, pp. 2903–2908, 2011.

[7] X. N. Gong, "Unloading behind of wall and earth pressure calculation," *Foundation Treatment*, vol. 6, no. 2, pp. 42-43, 1995.

[8] T. P. Qian, X. N. Gong, and Y. Li, "Analysis of braced excavation with pit-in-pit based on orthogonal experiment," *Applied Mechanics and Materials*, vol. 71–78, pp. 4549–4553, 2011.

[9] X. N. Gong, "Considerations on foundation pit engineering," *China Civil Engineering Journal*, vol. 38, no. 9, pp. 99–102, 2005.

[10] Z. Ding, J. Jin, and T.-C. Han, "Analysis of the zoning excavation monitoring data of a narrow and deep foundation pit in a soft soil area," *Journal of Geophysics and Engineering*, vol. 15, no. 4, pp. 1231–1241, 2018.

[11] C. Qi, J. Qi, L. Li, and J. Liu, "Stability analysis method for rock slope with an irregular shear plane based on interface model," *Advances in Civil Engineering*, vol. 2018, Article ID 8190908, 8 pages, 2018.

[12] R. Jedermann, C. Behrens, D. Westphal, and W. Lang, "Applying autonomous sensor systems in logistics-Combining sensor networks, RFIDs and software agents," *Sensors and Actuators A: Physical*, vol. 132, no. 1, pp. 370–375, 2006.

[13] J. B. Ong, Z. You, J. Mills-Beale, E. L. Tan, B. D. Pereles, and K. G. Ong, "A wireless, passive embedded sensor for real-time monitoring of water content in civil engineering materials," *IEEE Sensors Journal*, vol. 8, no. 11-12, pp. 2053–2058, 2008.

[14] N. Wang, N. Zhang, and M. Wang, "Wireless sensors in agriculture and food industry-Recent development and future perspective," *Computers and Electronics in Agriculture*, vol. 50, no. 1, pp. 1–14, 2006.

[15] W. R. Habel and K. Krebber, "Fiber-optic sensor applications in civil and geotechnical engineering," *Photonic Sensors*, vol. 1, no. 3, pp. 268–280, 2011.

[16] P. Lenke, S. Liehr, K. Krebber et al., "Distributed strain measurement with polymer optical fiber integrated in technical textiles using the optical time domain reflectometry technique," in *Proceedings of the 16th International POF Conference*, pp. 21–24, Turin, Italy, September 2007.

[17] M. Schallert, W. R. Habel, and D. Hofmann, "Analysis of concrete foundation piles using structure-integrated fiber-optic sensors," *TM-Technisches Messen*, vol. 75, no. 9, pp. 485–500, 2008.

[18] H. Xiao and J. Huang, "Experimental study of the applications of fiber optic distributed temperature sensors in detecting seepage in soils," *Geotechnical Testing Journal*, vol. 36, no. 3, article 20120096, 2013.

[19] A. Klar and R. Linker, "Feasibility study of automated detection of tunnel excavation by Brillouin optical time domain reflectometry," *Tunnelling and Underground Space Technology*, vol. 25, no. 5, pp. 575–586, 2010.

[20] H. Zhang and Z. S. Wu, "Performance evaluation of PPP-BOTDA-Based distributed optical fiber sensors," *International Journal of Distributed Sensors Newworks*, vol. 2012, no. 5, pp. 1497–1500, 2012.

[21] Z. G. Tao, C. Zhu, Y. Wang, W. Jiamin, H. Manchao, and Z. Bo, "Research on stability of an open-pit mine dump with fiber optic monitoring," *Geofluids*, vol. 2018, Article ID 9631706, 20 pages, 2018.

[22] M. He, W. Gong, J. Wang et al., "Development of a novel energy-absorbing bolt with extraordinarily large elongation and constant resistance," *International Journal of Rock Mechanics and Mining Sciences*, vol. 67, no. 67, pp. 29–42, 2014.

[23] Z. Tao, Y. Wang, C. Zhu et al., "Mechanical evolution of constant resistance and large deformation anchor cables and their application in landslide monitoring," *Bulletin of Engineering Geology and the Environment*, vol. 2019, no. 1, pp. 1–17, 2019.

[24] X.-m. Sun, Y. Zhang, D. Wang, J. Yang, H.-c. Xu, and M.-c. He, "Mechanical properties and supporting effect of CRLD bolts under static pull test conditions," *International Journal of Minerals, Metallurgy, and Materials*, vol. 24, no. 1, pp. 1–9, 2017.

[25] Z. Tao, C. Zhu, X. Zheng, and M. He, "Slope stability evaluation and monitoring of Tonglushan ancient copper mine relics," *Advances in Mechanical Engineering*, vol. 10, no. 8, article 168781401879170, 2018.

[26] Z. Tao, Z. Zhu, W. Han et al., "Static tension test and the finite element analysis of constant resistance and large deformation anchor cable," *Advances in Mechanical Engineering*, vol. 10, no. 12, article 168781401881063, 2018.

[27] J. Dai, M. Yang, X. Li, H. Liu, and X. Tong, "Magnetic field sensor based on magnetic fluid clad etched fiber Bragg grating," *Optical Fiber Technology*, vol. 17, no. 3, pp. 210–213, 2011.

[28] J. S. Leng and A. Asundi, "Non-destructive evaluation of smart materials by using extrinsic Fabry-Perot interferometric and fiber Bragg grating sensors," *NDT & E International*, vol. 35, no. 4, pp. 273–276, 2002.

[29] P. Shrestha, J.-H. Kim, Y. Park, and C.-G. Kim, "Impact localization on composite structure using FBG sensors and novel impact localization technique based on error outliers," *Composite Structures*, vol. 142, pp. 263–271, 2016.